RESEARCH ARTICLE

Key Points:
- The middepth oxygen-poor layer in the South Atlantic is salinity stratified
- This layer warms over the past few decades and freshens over the last decade
- This warming could result from very small changes in meridional velocities

Supporting Information:
- Supporting Information S1

Correspondence to:
D. Giglio,
dgiglio@ucsd.edu

Middepth decadal warming and freshening in the South Atlantic

Donata Giglio[1,2] and Gregory C. Johnson[3]

[1]Joint Institute for the Study of the Atmosphere and Ocean, University of Washington, Seattle, Washington, USA, [2]Now at Scripps Institution of Oceanography, University of California San Diego, La Jolla, California, USA, [3]NOAA/Pacific Marine Environmental Laboratory, Seattle, Washington, USA

Abstract South Atlantic Ocean middepth water property (temperature, salinity, oxygen, nutrients, etc.) distributions are set by salty, well-ventilated, and relatively nutrient-poor North Atlantic Deep Water (NADW) spreading southward toward the Southern Ocean underneath fresher, well-ventilated, and relatively nutrient-poor northward spreading Antarctic Intermediate Water (AAIW). The layer between the NADW and AAIW is oxygen-poor and nutrient-rich, with small vertical temperature gradients. Salinity stratification dominates the vertical density gradient, hence the layer is referred to as Salinity Stratified Layer (SSL). Decadal warming (0.044 °C decade^{-1}) and freshening (0.006 g kg^{-1} decade^{-1}) of this layer are analyzed using Argo data, a climatology, and repeat hydrographic sections. Warming within the SSL accumulates heat at a rate of ~20 TW, is unlikely to be caused by vertical heave, and is consistent with anomalous southward advection of order 10^2 km decade^{-1} in the Atlantic Meridional Overturning Circulation. Salinity changes within the SSL are consistent with a downward velocity anomaly of order 10 m decade^{-1}.

1. Introduction

Ocean warming in the Southern Hemisphere (SH) over the past few decades is prominent in both observations [*Gille*, 2008; *Sutton and Roemmich*, 2011; *Roemmich et al.*, 2015; *Wijffels et al.*, 2016] and model results [*Durack et al.*, 2014]. This warming provides the largest contribution to global ocean heat content changes, in part due to the larger volume of water in the SH compared to its northern counterpart [*Durack et al.*, 2014]. However, observations in the SH have been historically sparse until the advent of Argo profiling floats [*Riser et al.*, 2016] and earlier estimates of SH ocean heat uptake are likely biased low [*Durack et al.*, 2014].

Ocean heat uptake is key to understanding how Earth's climate is evolving [*Rhein et al.*, 2013], with ocean circulation regulating heat redistribution in the climate system [*Talley*, 2003]. A maximum in ocean warming is observed at 40°S, near the center of the subtropical gyres' deep portion in the three oceans [*Roemmich et al.*, 2015]. This heat gain is consistent with subduction of heat by the mean circulation and a continued strengthening of the subtropical gyres [*Roemmich et al.*, 2007] arising from changes in the pattern and strength of midlatitude westerly winds. Also, the vertical structure of ocean warming in the 500–2000 m range shows a broad maximum between 700 and 1400 m [*Roemmich et al.*, 2015], corresponding to warming intermediate water layers [*Schmidtko and Johnson*, 2012]. These waters form at high southern latitudes, subduct, and carry their temperature and salinity (Θ – S$_A$) properties equatorward, through the subtropical gyre interior.

The South Atlantic is one of the regions where ocean warming has been underestimated, especially previous to the Argo program [*Durack and Wijffels*, 2010; *Durack et al.*, 2014]. Even coverage of Argo profiling floats is sparser there compared to other ocean basins [*Riser et al.*, 2016]. Yet the South Atlantic circulation includes subtropical and sub polar gyres, a portion of the Antarctic Circumpolar Current (ACC), and the North Atlantic and Antarctic branches of the Meridional Overturning Circulation (MOC). It also plays an important role in heat redistribution in the climate system [*Talley*, 2003]. Distributions of middepth water properties in the South Atlantic Ocean [*Tsuchiya et al.*, 1994] are different from those of the South Indian and South Pacific oceans, due to salty North Atlantic Deep Water (NADW) spreading southward toward the Southern Ocean (SO) underneath fresher Antarctic Intermediate Water (AAIW), spreading northward from
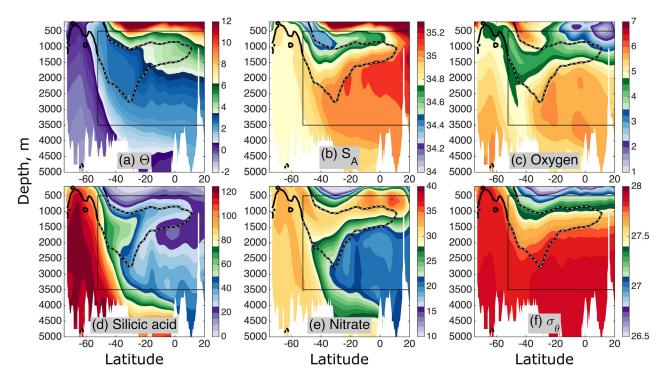
Figure 1. WOCE climatology section along 22.5°W in the South Atlantic Ocean. (a) Conservative temperature (°C), (b) Absolute salinity (g kg^{-1}), (c) Oxygen (ml l^{-1}), (d) Silicic–acid (μ mol kg^{-1}), (e) Nitrate (μ mol kg^{-1}), and (f) Potential Density (kg m^{-3}). Thick black contours indicate zero Turner angle and are partially overlayed by the gray dashed line which bounds the Salinity Stratified Layer (SSL) north of the Polar Front (southern side of black box), and below the 500 m isobath (top side of black box).

the SO. The layer between the NADW and AAIW is weakly ventilated, hence oxygen-poor, and nutrient-rich. It can be characterized by vertical temperature gradients much weaker than its vertical salinity gradients, making it an interesting place to diagnose warming trends. This layer includes Upper Circumpolar Water (UCPW) south of ∼22°S [*Tsuchiya et al.*, 1994].
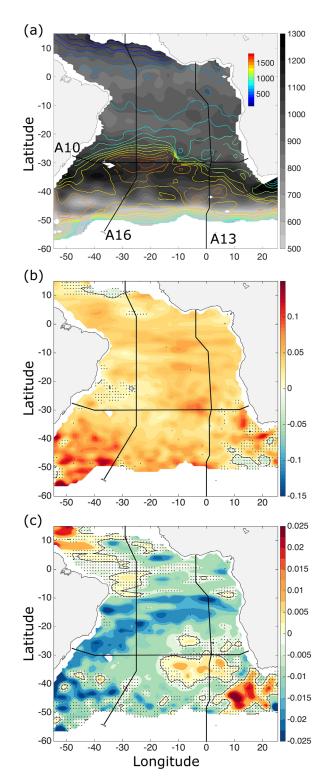
Here we describe the mean and time-varying Θ–S_A properties of this layer in the South Atlantic Ocean at depths greater than 500 m. We use Argo observations, a World Ocean Circulation Experiment (WOCE) climatology, and repeat hydrographic section data. We also discuss how ocean circulation changes may relate to the observed warming signal. Section 2 describes the data and section 3 the methods. SSL time mean properties are presented in section 4.1, while SSL Θ–S_A variability from Argo and hydrographic section data are in section 4.2. Section 5 presents the summary and conclusions.
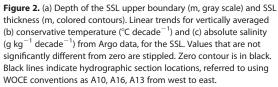
2. Data

We use the WOCE Global Hydrographic Climatology [*Gouretski and Koltermann*, 2004] to define the layer of interest. This climatology consists of optimally analyzed gridded fields of temperature, salinity, dissolved oxygen, and nutrients with 0.5° spatial resolution (Figure 1). It is based on in-situ observations of the global ocean between 1990 and 1998, with selected data from several earlier cruises included as well.

Argo temperature and salinity profiles provide global in situ (0–2000 db) ocean observations north of about 60°S, with unprecedented sampling of the South Atlantic [*Roemmich et al.*, 2009]. We use objectively mapped monthly fields [*Roemmich and Gilson*, 2009] on a 1 × 1 degree grid, constructed from Argo Θ–S_A observations during 2006–2015, after quality control and adjustment of pressure bias.

We use hydrographic data collected from ships in the past four decades to estimate long-term Θ–S_A trends along the path of WOCE sections (Figure 2) A10 (occupied in 1993, 2003, 2011), A13.5 (occupied in 1983/1984 and 2010), and A16 (occupied in 1989, 2005, and 2014).

Figure 2. (a) Depth of the SSL upper boundary (m, gray scale) and SSL thickness (m, colored contours). Linear trends for vertically averaged (b) conservative temperature (°C decade^{-1}) and (c) absolute salinity (g kg^{-1} decade^{-1}) from Argo data, for the SSL. Values that are not significantly different from zero are stippled. Zero contour is in black. Black lines indicate hydrographic section locations, referred to using WOCE conventions as A10, A16, A13 from west to east.

3. Methods

The layer of interest (hereafter the SSL, for Salinity Stratified Layer) is located in the South Atlantic, at depths greater than 500 m, and is characterized by small vertical gradients in temperature (Figure 1a). We define the SSL using the WOCE climatology (Figure 1) as the region with negative Turner angle [*Ruddick*, 1983] that is north of the ACC Polar Front [*Giglio and Johnson*, 2015] and deeper than 500 m. The Turner angle is defined as $Tu = \tan^{-1}\left(\alpha\frac{\partial\Theta}{\partial z} - \beta\frac{\partial S_A}{\partial z}, \alpha\frac{\partial\Theta}{\partial z} + \beta\frac{\partial S_A}{\partial z}\right)$ [*Ruddick*, 1983; *McDougall et al.*, 1988], with α and β the thermal expansion and the saline contraction coefficients, respectively. A negative Turner angle indicates a smaller contribution to the buoyancy frequency from the conservative temperature (Θ) vertical gradient than from the absolute salinity (S_A) vertical gradient. Hence, within the SSL the vertical gradient of salinity dominates the buoyancy frequency (i.e., the density stratification, Figures 1a, 1b, and 1f).

SSL variability is quantified in the following analysis based on Θ and S_A trends. Uncertainties of spatially averaged trends are computed as standard errors, i.e., $\epsilon = \frac{\sigma}{\sqrt{n}}$, with σ the standard deviation, and n the number of independent grid points in the average. For instance, when averaging trends in the 3D SSL, only areas of 10 points in longitude by 5 points in latitude are considered to be independent. SSL heat and freshwater changes are also considered in the following, and calculations are based on a fixed SSL volume estimated using the WOCE climatology.

4. Results

4.1. SSL Time Mean Properties

The SSL is weakly ventilated, hence oxygen-poor (Figure 1c) and nutrient-rich (Figure 1d, 1e), and is further characterized by small vertical gradients in temperature (Figure 1a, section 3). The SSL shows the greatest thickness ($\sim$1700 dbar) and depths in the subtropical gyre (30 – 35°S at 35 – 8°W, Figure 2a), with its upper boundary shoaling to the south, and extends as far north as 15°N in the western part of the South Atlantic. The SSL is thicker than 1000 m in the latitude band 50 – 40°S, where its upper boundary is shallower than 1000 m.

South of $\sim$22°S, the main water mass within the SSL is UCPW [*Tsuchiya et al.*, 1994], an

old, poorly ventilated mixture of several different water masses (AAIW, NADW, AABW, Pacific and Indian Deep Waters, etc.). The oxygen minimum associated with UCPW reaches the South Atlantic from the Pacific Ocean through Drake Passage [*Callahan*, 1972; *Gordon and Molinelli*, 1982; *Peterson and Whitworth*, 1989] and lies below the oxygen maximum of the AAIW. Oxygen concentrations within the minimum are lowest south of 40°S, increasing northward to 30°S from mixing with the overlying and underlying waters in the subtropical gyre [*Tsuchiya et al.*, 1994]. North of 22°S, the oxygen-poor water within the SSL is part of the equatorial oxygen minimum and comes from the eastern South Atlantic [*Reid*, 1989]. A silicic–acid maximum is found at nearly the same depths as the oxygen minimum starting at the Polar Front and extending northward [*Tsuchiya et al.*, 1994]. However, the density of this maximum shifts lighter suddenly around 22°S as a result of eastward flow of nutrient-poor NADW [*Talley and Johnson*, 1994]. As a result of this shift, the silicic-acid maximum is near the core of the AAIW (and not UCPW) north of 22°S [*Tsuchiya et al.*, 1994]. At the silicic-acid maximum, conservative temperature is highly uniform both horizontally and vertically ($\sim$2.6°C, Figures 1a and 1d) [*Tsuchiya et al.*, 1994]. Waters with similar characteristics are present in a large amount in the South Pacific [*Montgomery*, 1959] and may originate there [*Tsuchiya et al.*, 1994]. To the north and south of this uniform region (and in general within the SSL) vertical gradients of conservative temperature remain weak. However, there are substantial meridional gradients of conservative temperature within the SSL.

4.2. SSL Warming and Freshening

An ocean basin-wide warming trend with a mean value of 0.044 $\pm$0.001 °C decade^{-1} is observed within the SSL during 2006–2015 from Argo (Figure 2b), with a stronger signal in the south part of the basin. Temperature variability in the SSL is very well described by a linear trend that weakens somewhat with increasing depth (supporting information Figure S1). Freshening at a mean rate of 0.006 $\pm$ 0.0003 g kg^{-1} decade^{-1} is also observed since 2006 and above 2000 dbar (within the SSL, Figure 2c), with stronger signals in the south tropics and in the southwest portion of the SSL region. Increasing salinity is observed in the west tropical region equatorward of $\sim$10° latitude and in the east, south of $\sim$30°S (Figure 2c and supporting information Figure S2b). Interannual variability is strong in the SSL salinity time series (Figure S1b).

The Argo array measures as deep as 2000 dbar, hence shallower than the SSL in some regions of the South Atlantic (Figures 2a and 3). However, hydrographic data along a few decadally reoccupied sections that cross the SSL (Figure 2b) show that the warming has persisted throughout the SSL for the past few decades including below the present 2000–dbar pressure limit of Argo (Figures 3c, 4a, and 4d, for pressure levels deeper than $\sim$1000 dbar; similar and not shown for the A10 and A13 sections). The freshening observed during Argo does not appear to extend back to the 1980s (Figure 3b versus Figures 3d and Figure 4b; not shown for the A10 and A13 sections), although interannual salinity variations in the SSL may be aliased by the section sampling. Nonetheless, trends from hydrography are consistent with Argo results of decreasing salinity if we only use post-2003 hydrographic data (Figure 4e). Post-2003, section A16 was occupied fully only in 2005 and 2014. Yet as these sections afford averaging spatially over many mesoscale eddies, the results tend to be robust. Furthermore, the consistency of the comparison with Argo reinforces the repeat hydrography results.

The SSL warming (and hence, by definition, salinification) is observed also on isopycnals within the SSL (Figures 4c, 4f, 4g, and 4h, for pressure levels deeper than $\sim$1000 dbar and isopycnals denser than $\sim$27.3 kg/m^3).

5. Summary and Discussion

The SSL is an oxygen-poor, nutrient-rich region characterized by very weak vertical gradients in conservative temperature. Argo data show that the SSL has been warming and (overall) freshening during 2006–2015. The warming weakens with increasing depth, slightly increasing vertical temperature stratification in the SSL. Yet resulting SSL volume changes during the period of interest are very small (e.g., order 10 m in depth) and not well constrained with the available Argo observations. These changes are also difficult to interpret (e.g., in relation to a southward transport) since information at the boundaries is not available. The warming within the portion of the SSL shallower than 2000 dbar integrates to $\sim$20 TW rate of heat gain, about 6% of the net ocean heating rate of $\sim$350 TW [e.g., *Johnson et al.*, 2016]. The warming also extends below the 2000-dbar sampling limit of Argo and has been occurring over the past few decades, as measured by hydrographic data. However, hydrographic data show freshening in the SSL pressure range only
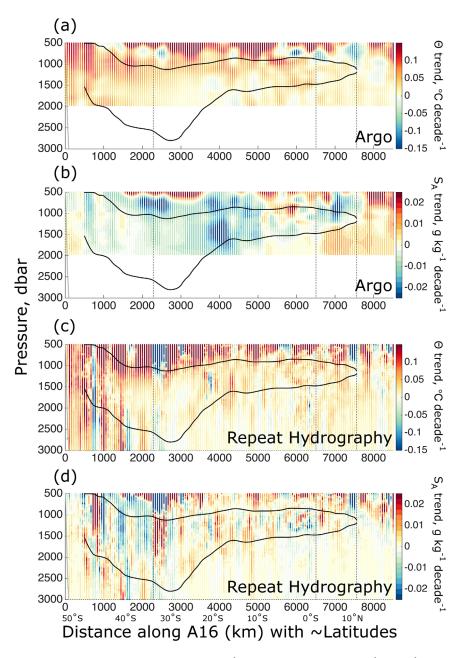
Figure 3. Linear trends in (a, c) conservative temperature (°C decade^{-1}), and (b, d) absolute salinity (g kg^{-1} decade^{-1}) along A16 (Fig. 2) using (a, b) Argo, and (c, d) repeat hydrographic section data. Vertical dashed lines indicate where the section changes direction. The SSL boundary (north of the ACC Polar Front) is indicated in black, and bathymetry in gray. *X* axis is distance along-section from south to north, with the approximate latitudes indicated in the bottom plot.

post-2003. This freshening is stronger in the south tropics and western south subtropics, with positive trends in salinity in the east of the South Atlantic south of ~30°S, possibly related to an increased Agulhas leakage [*Beal et al.*, 2011]. Warming is observed also on potential density surfaces.

The warming in the SSL could be owing to a change in velocities acting in conjunction with lateral gradients; mixing of warmth from above, below, or laterally; or a change in temperature (and salinity) where the middepth isopycnals outcrop, at higher latitudes. Hence, the causes of the warming are not easy to diagnose. The one possibility that can be discounted is isopycnal heave, because the vertical temperature gradients within the SSL are so small. Vertical mixing of anomalously warm waters at the upper boundary of the SSL, notably AAIW [*Schmidtko and Johnson*, 2012], or its lower boundary may play a role. However, even assuming a relatively large vertical mixing coefficient, warming by this mechanism would not be enough alone
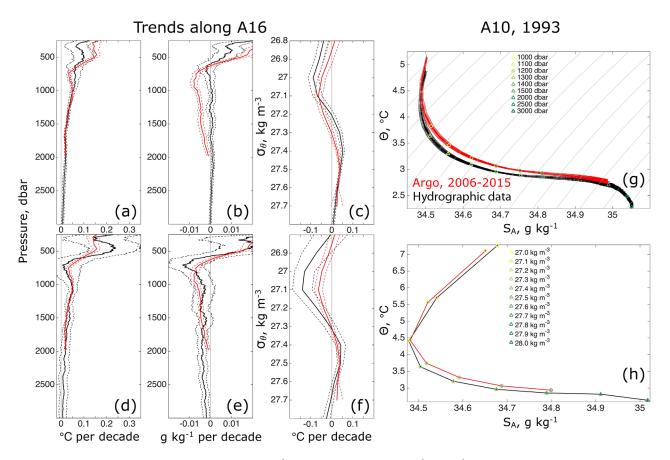
Figure 4. (a–f) Linear trends in (a, c, d, f) conservative temperature (°C decade^{-1}), and (b, e) absolute salinity (g kg^{-1} decade^{-1}) averaged along the A16 section. Trends from Argo during 2006 to 2015 (red). Trends from hydrographic data (a–c) using all the profiles available (from 1989 to 2014) and (d–f) only post-2003 data (black). Dashed lines indicate errorbars. The y axis is (a, b, d, e) pressure or (c, f) potential density. (g, h) $\Theta - S_A$ diagrams averaged along the A10 section, from hydrographic (black, for 1993) and Argo (red, for 2006–2015) data on (g) pressure and (h) potential density surfaces. Errorbars are also shown. Gray lines in (g) represent different isopycnals.

to reproduce the observed temperature trends within SSL (not shown). Also, the SSL is oxygen-poor (Figure 1c), and hydrographic sections do not show an increase in oxygen within the SSL over the past few decades. Hence, ventilation by increased mixing with AAIW or NADW may not contribute much to the warming.

The average warming rate in the SSL (i.e., order 10^{-2} °C decade^{-1}, from Argo) is consistent with anomalous southward advection of the time mean meridional temperature gradient (i.e., order 10^{-4} °C km^{-1}), with a southward velocity anomaly of order 10^2 km decade^{-1} (i.e., 10^{-1} mm s^{-1}). This diagnosis would imply changes in the AMOC transport on the order of 1 Sv (10^6 m^3 s^{-1}) either in terms of strength or vertical structure of the stream function, since the AMOC upper cell transport reverses (from southward to northward) within the SSL [*Marshall and Speer*, 2012; *Lumpkin and Speer*, 2007]. AMOC variability may occur as a result of changes in the winds over the South Atlantic or water mass formation in the North Atlantic [*Johnson and Marshall*, 2002]. Yet *Johnson and Marshall* [2002] show how only low-frequency forcing in either of the basins affects the AMOC stream function in the other. Sustaining the SAMBA array [*Ansorge et al.*, 2014] over time will provide unprecedented observations to relate future changes in the SSL to AMOC variability.

Finally, because the vertical gradient of absolute salinity is large within the SSL, freshening within the SSL could be a result of isopycnal heave. The average freshening rate on pressure surfaces in the SSL (i.e., order 10^{-3} g kg^{-1} decade^{-1}, from Argo) is consistent with anomalous downward advection of the time mean vertical S_A gradient (i.e., order 10^{-4} g kg^{-1} m^{-1}), with a downward vertical velocity anomaly of order 10 m decade^{-1}. This estimate is based solely on the observed salinity tendency and may be biased low, since the anomalous meridional advection of the time mean meridional gradient would tend to increase salinity.

The Argo array provides an unprecedented database to study changes in ocean heat and freshwater content and distribution especially in the SH. Also, volume-averaged property changes, or water-mass changes,

can be used to infer variations that are difficult to detect with velocity measurements. Yet the core Argo array is limited to the upper 2000 m. While repeat hydrographic sections will continue to be a cornerstone of the deep ocean observing system, providing reference temperature and salinity data as well as biogeochemical data with synoptic eddy-resolving sampling at decadal intervals [*Talley et al.*, 2016], the implementation of a deep Argo array [*Johnson et al.*, 2015] will allow better-sampled assessments of water-property changes below the sampling depth of Argo on shorter than decadal time scales, which will become increasingly important as the deep ocean is increasingly impacted by climate change [*Gleckler et al.*, 2016].

References

Ansorge, I. J., et al. (2014), Basin-wide oceanographic array bridges the South Atlantic, *Eos Trans. AGU*, *95*(6), 53–54, doi:10.1002/2014EO060001.

Beal, L. M., W. P. M. De Ruijter, A. Biastoch, and R. Zahn (2011), On the role of the Agulhas system in ocean circulation and climate, *Nature*, *472*(7344), 429–436.

Callahan, J. E. (1972), The structure and circulation of deep water in the Antarctic, *Deep Sea Res. Oceanogr. Abstr.*, *19*(8), 563–575.

Durack, P. J., and S. E. Wijffels (2010), Fifty-year trends in global ocean salinities and their relationship to broad-scale warming, *J. Clim.*, *23*(16), 4342–4362, doi:10.1175/2010JCLI3377.1.

Durack, P. J., P. J. Gleckler, F. W. Landerer, and K. E. Taylor (2014), Quantifying underestimates of long-term upper-ocean warming, *Nat. Clim. Change*, *4*(11), 999–1005.

Giglio, D., and G. C. Johnson (2015), Subantarctic and polar fronts of the Antarctic Circumpolar Current and Southern Ocean heat and freshwater content variability: A view from Argo, *J. Phys. Oceanogr.*, *46*(3), 749–768, doi:10.1175/JPO-D-15-0131.1.

Gille, S. T. (2008), Decadal-scale temperature trends in the Southern Hemisphere Ocean, *J. Clim.*, *21*(18), 4749–4765, doi:10.1175/2008JCLI2131.1.

Gleckler, P. J., P. J. Durack, R. J. Stouffer, G. C. Johnson, and C. E. Forest (2016), Industrial-era global ocean heat uptake doubles in recent decades, *Nat. Clim. Change*, *6*, 394–398.

Gordon, A., and E. Molinelli (1982), Thermohaline and chemical distributions and the atlas data set, in *Southern Ocean Atlas*, pp. 1–11 and 233, Columbia Univ. Press, New York.

Gouretski, V., and K. Koltermann (2004), *WOCE Global Hydrographic Climatology*, 35/2004, Ber. des Bundesamtes fur Seeschifffahrt und Hydrogr, Hamburg, Germany. [Available at http://icdc.zmaw.de/1/daten/ocean/woce-climatology.html.]

Johnson, G. C., J. M. Lyman, and S. G. Purkey (2015), Informing deep Argo array design using Argo and full-depth hydrographic section data, *J. Atmos. Oceanic Technol.*, *32*(11), 2187–2198, doi:10.1175/JTECH-D-15-0139.1.

Johnson, G. C., J. M. Lyman, and N. G. Loeb (2016), Improving estimates of earth's energy imbalance, *Nat. Clim. Change*, *6*(7), 639–640.

Johnson, H. L., and D. P. Marshall (2002), Localization of abrupt change in the North Atlantic thermohaline circulation, *Geophys. Res. Lett.*, *29*(6), 1083, doi:10.1029/2001GL014140.

Lumpkin, R., and K. Speer (2007), Global ocean meridional overturning, *J. Phys. Oceanogr.*, *37*(10), 2550–2562, doi:10.1175/JPO3130.1.

Marshall, J., and K. Speer (2012), Closure of the meridional overturning circulation through Southern Ocean upwelling, *Nat. Geosci.*, *5*(3), 171–180.

McDougall, T. J., S. A. Thorpe, and C. H. Gibson (1988), *Small-Scale Turbulence and Mixing in the Ocean: A Glossary*, vol. 46, pp. 3–9, Elsevier, Amsterdam, doi:10.1016/S0422-9894(08)70533-6.

Montgomery, R. B. (1959), Water characteristics of Atlantic Ocean and of world ocean, *Deep Sea Res.*, *5*(2), 134–148.

Peterson, R. G., and T. Whitworth (1989), The subantarctic and polar fronts in relation to deep water masses through the southwestern Atlantic, *J. Geophys. Res.*, *94*(C8), 10,817–10,838, doi:10.1029/JC094iC08p10817.

Reid, J. L. (1989), On the total geostrophic circulation of the South Atlantic ocean: Flow patterns, tracers, and transports, *Prog. Oceanogr.*, *23*(3), 149–244.

Rhein, M., et al. (2013), Observations: Ocean, in *Climate Change 2013: The Physical Science Basis. Contribution of Working Group I to the Fifth Assessment Report of the Intergovernmental Panel on Climate Change*, Cambridge Univ. Press, Cambridge, U. K, New York.

Riser, S. C., et al. (2016), Fifteen years of ocean observations with the global Argo array, *Nat. Clim. Change*, *6*(2), 145–153.

Roemmich, D., and J. Gilson (2009), The 2004–2008 mean and annual cycle of temperature, salinity, and steric height in the global ocean from the Argo program, *Prog. Oceanogr.*, *82*(2), 81–100, doi:10.1016/j.pocean.2009.03.004.

Roemmich, D., J. Gilson, R. Davis, P. Sutton, S. Wijffels, and S. Riser (2007), Decadal spinup of the South Pacific subtropical gyre, *J. Phys. Oceanogr.*, *37*(2), 162–173, doi:10.1175/jpo3004.1.

Roemmich, D., G. Johnson, S. Riser, R. Davis, J. Gilson, W. Owens, S. Garzoli, C. Schmid, and M. Ignaszewski (2009), The Argo program: Observing the global ocean with profiling floats, *Oceanography*, *22*(2), 34–43.

Roemmich, D., J. Church, J. Gilson, D. Monselesan, P. Sutton, and S. Wijffels (2015), Unabated planetary warming and its ocean structure since 2006, *Nat. Clim. Change*, *5*(3), 240–245.

Ruddick, B. (1983), A practical indicator of the stability of the water column to double-diffusive activity, *Deep Sea Res. Part A*, *30*(10), 1105–1107, doi:10.1016/0198-0149(83)90063-8.

Schmidtko, S., and G. C. Johnson (2012), Multidecadal warming and shoaling of Antarctic Intermediate Water*, *J Clim.*, *25*(1), 207–221, doi:10.1175/JCLI-D-11-00021.1.

Sutton, P., and D. Roemmich (2011), Decadal steric and sea surface height changes in the Southern Hemisphere, *Geophys. Res. Lett.*, *38*, L08604, doi:10.1029/2011GL046802.

Talley, L. D. (2003), Shallow, Intermediate, and deep overturning components of the global heat budget, *J. Phys. Oceanogr.*, *33*(3), 530–560.

Talley, L. D., and G. C. Johnson (1994), Deep, zonal subequatorial currents, *Science*, *263*(5150), 1125–1128.

Talley, L. D., et al. (2016), Changes in ocean heat, carbon content, and ventilation: A review of the first decade of GO-SHIP global repeat hydrography, *Annu. Rev. Mar. Sci.*, *8*, 185–215, doi:10.1146/annurev-marine-052915-100829.

Tsuchiya, M., L. Talley, and M. McCartney (1994), Water-mass distributions in the western South Atlantic; a section from South Georgia island (54°S) northward across the equator, *J. Mar. Res.*, *52*, 55–81.

Wijffels, S., D. Roemmich, D. Monselesan, J. Church, and J. Gilson (2016), Ocean temperatures chronicle the ongoing warming of earth, *Nat. Clim. Change*, *6*(2), 116–118.